Bulgarian Chemical Communications, Volume 58, Special Issue A (pp. 59-64) 2026 DOI: 10.34049/bcc.58.A.SN-11

Comparative study of the textural properties of chitosan, zeolite and their composite membrane

K. Zafirova[1], L. Gonsalvesh[2], D. Zvezdova[3*]

[1]*Medical University "Prof. Dr. Paraskev Stoyanov", Faculty of Pharmacy, Varna, Bulgaria*
[2]*Burgas State University "Prof. Dr. Assen Zlatarov", Faculty of Natural Sciences, Burgas, Bulgaria*
[3]*Burgas State University "Prof. Dr. Assen Zlatarov", Faculty of Public Health and Health Care, Burgas, Bulgaria*

Received: September 04, 2025; Revised: November 11, 2025

A comparative analysis was conducted to evaluate the textural properties of chitosan, zeolite and their composite membrane based on nitrogen adsorption data. Zeolite exhibited the highest specific surface area (25 m^2/g) and total pore volume (0.0964 cm^3/g), while chitosan showed limited porosity with predominantly mesoporous structure. The composite membrane demonstrated intermediate characteristics (5 m^2/g, 0.0238 cm^3/g), reflecting a successful structural integration that enhances its functional performance relative to the individual components.

Keywords: Chitosan–zeolite composite membrane, Porosity, FTIR, SEM

INTRODUCTION

Chitosan (CS), a polycationic biopolymer and waste product from seafood processing industry, is the second most abundant natural polysaccharide after cellulose. Some of the most noted properties of CS are biocompatibility, biodegradability, non-toxicity, adsorption properties, etc. In medical field, chitosan films have been tested as curative wound dressing and as scaffolds for tissue and bone engineering [1]. However, CS has low mechanical properties and is soluble in acidic media, which limits its application as an adsorbent at low pH [2]. In order to overcome these limitations, physical and chemical modification needs to be carried out on chitosan by its immobilization on a low-cost material such as zeolite. The combination of zeolite with a polymer backbone was found to lead to improved strength and heat resistance [3].

Studies have been conducted on the textural characteristics, characterization methods, and specific surface area values of porous materials derived from various sources for obtaining chitosan and its composite structures [4-8].

Over the last decades, biopolymer–zeolite hybrid materials which are known to combine physical and chemical properties of both inorganic and organic materials have gained increasing attention in the areas of science and technology of biopolymer-based advanced materials [9-13]. Infection by pathogenic microorganisms remains a major challenge in wound treatment. Natural polymers such as chitosan exhibit broad-spectrum antibacterial activity making them suitable for wound dressings. However, their low mechanical strength and water-retention capacity limit practical use. Zeolites, microporous aluminosilicates with ion-exchange capacity and antimicrobial potential, have been proposed as reinforcing agents to improve the performance of biopolymer-based materials. This material appears as a promising support due to its mechanical strength and chemical stability, low cost, and availability [9].

CSZ composites have been used in medical fields [14, 15]. It is well known that a surface interaction between CS and Z induces changes in microstructure morphology and surface chemistry, which are fundamental in adsorption processing, and for drug delivery process. Their combination with chitosan represents a promising strategy to enhance material properties through complementary interactions. This study presents a comparative analysis of the porous structure of chitosan, zeolite and a chitosan–zeolite composite membrane, aiming to evaluate the influence of composition on textural parameters.

EXPERIMENTAL

Chitosan (CS) was extracted from Black Sea shrimp shells through standard chemical treatment involving demineralization with hydrochloric acid, deproteinization with sodium hydroxide, and deacetylation in concentrated alkali solution. Natural zeolite (Z), identified as clinoptilolite, was used as received.

The procedure involves the preliminary preparation of a chitosan–zeolite (CSZ) membrane by combining a 1% chitosan solution (prepared by

* To whom all correspondence should be sent:
E-mail: *zvezdova@abv.bg*

dissolving 1 g of chitosan in 100 mL of 1% acetic acid at 52°C under continuous magnetic stirring for 24 h) with a 0.5% aqueous zeolite (clinoptilolite) suspension. The resulting chitosan–zeolite mixture was subsequently poured into Petri dishes and dried at 60°C to obtain uniform membranes.

Porous structure characterization was carried out using nitrogen adsorption isotherms at 77 K on a Surfer apparatus (Thermo Scientific). Specific surface area was calculated *via* the BET method (ISO 9277:2010). Total pore volume was obtained from the desorption branch at P_i/P_0 = 0.95, while micropore volume was evaluated using the Dubinin-Radushkevich equation. Pore size distribution was determined by applying NLDFT using the n2si77K_cyl kernel (ISO 15901-3:2007).

RESULTS AND DISCUSSION

Scanning electron microscopy (SEM) studies were carried out on the surfaces of chitosan (CS) and chitosan/zeolite nanocomposite films (CSZ). For the SEM analyses, in order to ensure sample conductivity, the specimens were gold-coated using a standard metallization procedure. The surface morphology of the CSZ films, as well as the mechanophysical structure of the studied materials, is presented in Figures 1 and 2.

The rough, uneven surface of the CSZ film may be due to loosely bound zeolite particles that were not fully and evenly dispersed within the formed nanocomposite film, owing to their poor solubility in water. The samples were examined using a scanning electron microscope (SEM) equipped with an X-ray microanalyzer (XMA). Digital micrographs in secondary electron mode were taken during the observations. The results of the surface examinations are presented in Figs. 1–5.

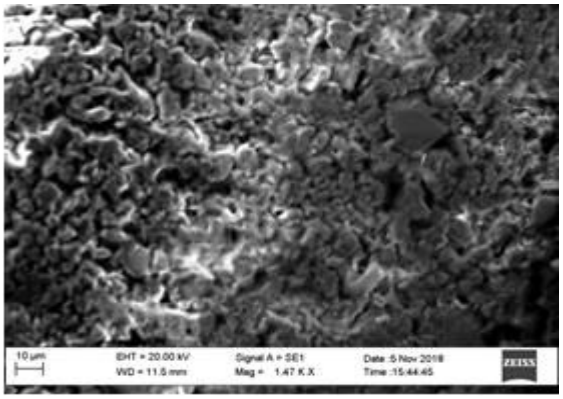

Fig. 1. Surface of a chitosan/ zeolite nanocomposite biofilm (×1470)

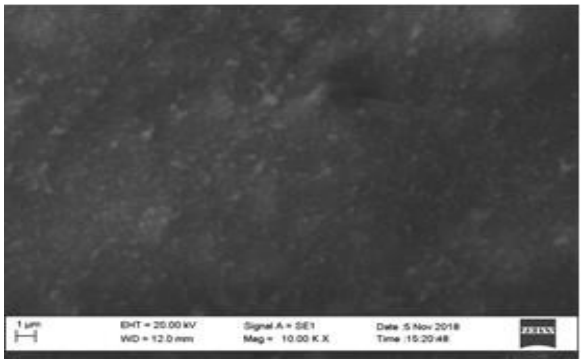

Fig. 2. Surface of a pure chitosan biofilm (×10,000)

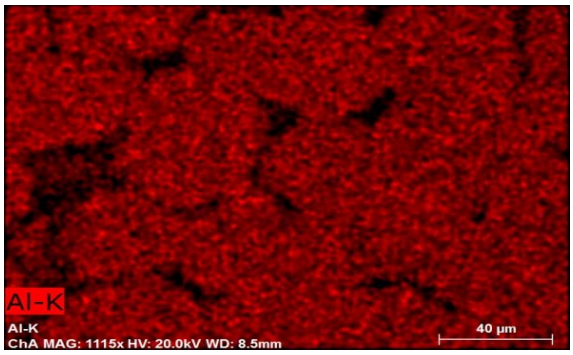

Fig. 3. Distribution of aluminum over the area, XMA, characteristic X-ray radiation – Al Kα

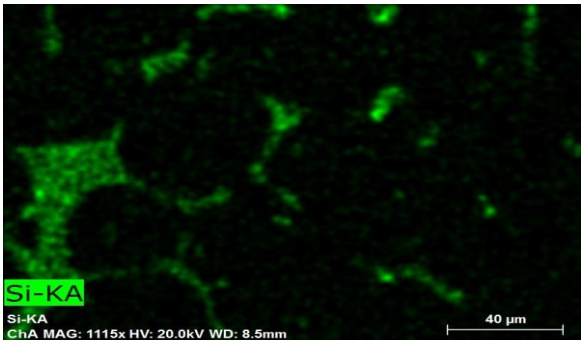

Fig. 4. Distribution of silicon over the area, XMA, characteristic X-ray radiation – Si Kα

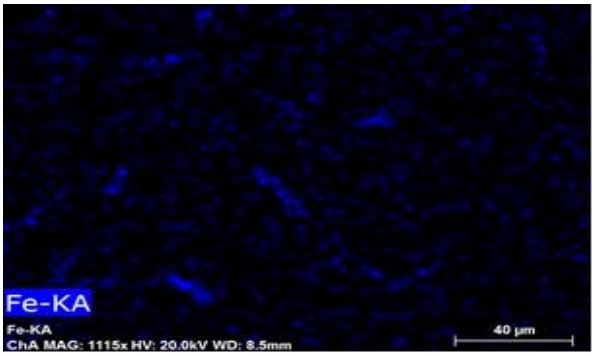

Fig. 5. Distribution of iron over the area, XMA, characteristic X-ray radiation – Fe Kα

In the samples of the chitosan/zeolite nanocomposite biofilm and the pure chitosan biofilm, two distinct types of surface structures can be observed. Terminologically, this classification defines two main types of mechanophysical structures: with distinct mechanophysical porosity (polyreticular non-gel porous type – Fig. 1) and without distinct mechanophysical porosity (gel type – Fig. 2). The figures show that, even at a magnification of 1470×, the chitosan/zeolite nanocomposite biofilm exhibits a mechanophysical porous structure (Fig. 1), whereas the second type, even at a magnification of ×10,000 displays a uniform, smooth, nonporous gel-type structure (Fig. 2).

From Fig. 1, a variation can be observed in the size of the elements forming the individual sections of the structure of the chitosan/zeolite nanocomposite biofilm. Fig. 3 shows an area located between the two types of surfaces. The surface morphology of the gel sample (Fig. 2) corresponds to the second type of structure (gel type). This structure is more uniform, without a distinct porous relief. For the chitosan/zeolite nanocomposite biofilm sample, the chemical composition was examined using an X-ray microanalyzer (XMA) on a cross-sectional cut of the sample. The results regarding the distribution of the elements Al, Si, and Fe are presented in Table 1 and in Figs. 3–5.

Analyses were performed using area scanning, from which the average composition of the sample was obtained, as well as point analyses for several zones. The results, with relatively good approximation, correspond to the presented area distribution.

Table 1. Chemical composition of Al, Si, and Fe in chitosan/zeolite nanocomposite biofilm

Element	Average composition, %	Zone 1, %	Zone 2, %
Al	97.18	85.02	83.59
Si	22.60	21.82	21.41
Fe	3.14	3.16	3.01

FTIR spectra of zeolite (Z) films and chitosan-zeolite nanocomposite (CSZ) films are shown in Figure 6. The spectrum of CS exhibits a broad peak at 3431.81 cm^{-1}, reflecting vibrational modes characteristic of NH and OH groups, at 2921 cm^{-1} (C–H symmetric stretching), at 1378.7 cm^{-1}, at 1654.9 cm^{-1} (amide II and C=O groups), at 1420 cm^{-1} (H–H vibrations), at 1152.6 cm^{-1} (C–O–C vibration), and at 1081.4 cm^{-1} (C–OH).

As shown in Figure 6(a), the FTIR spectrum of Z exhibits a peak at 1636.4 cm^{-1}, attributed to Si–O–Si bonding. Additionally, characteristic absorption peaks are observed at 1636 cm^{-1} (H–O–H), 794.5 cm^{-1} (Al–Al–OH bending vibration), and 467 cm^{-1} (Si–O). The spectrum of the CSZ nanocomposite film [Figure 6(b)] shows a characteristic band at 3431.8 cm^{-1}, which is due to hydrogen bonding formation between the functional groups of CS (O–H and N–H groups) and Z (O–H groups). The peak observed in the CS spectrum at 1654.9 cm^{-1} shifts to 1644.1 cm^{-1} in the CSZ spectrum [Figure 6(a)], corresponding to the deformation vibration of the amino groups of chitosan.

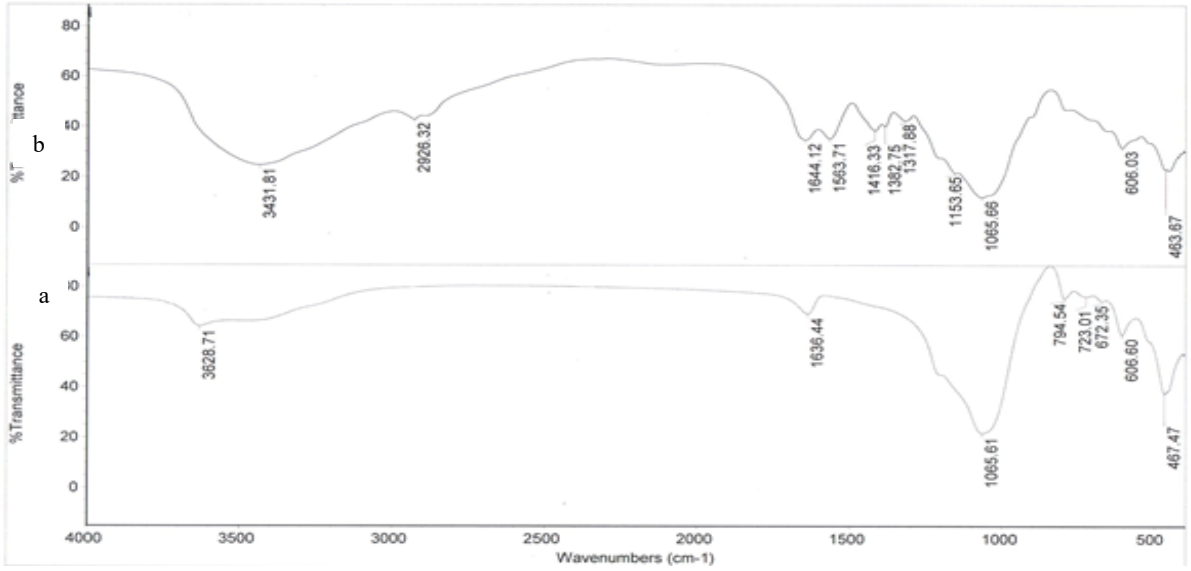

Fig. 6. FTIR spectra of zeolite (a) and chitosan-zeolite composite (b).

Porous structure of biomaterials may significantly vary depending on the used precursor and processing technology. Inasmuch as porous structure of a certain material determines its beneficial specific application, the proper porous texture evaluation and characterization is important. Porous characteristics of the bio-chars under consideration can be deduced from the N_2 adsorption isotherms presented on Figs. 7, 9, 11. Pore size distributions of zeolite, chitosan and chitosan-zeolite composite are shown in Figs. 8, 10, 12.

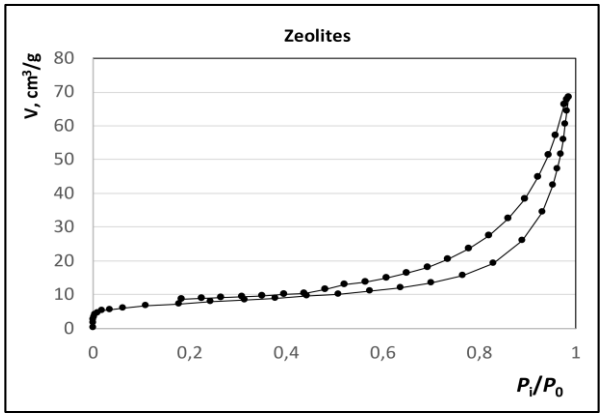

Fig. 7. N_2 adsorption isotherms of zeolite.

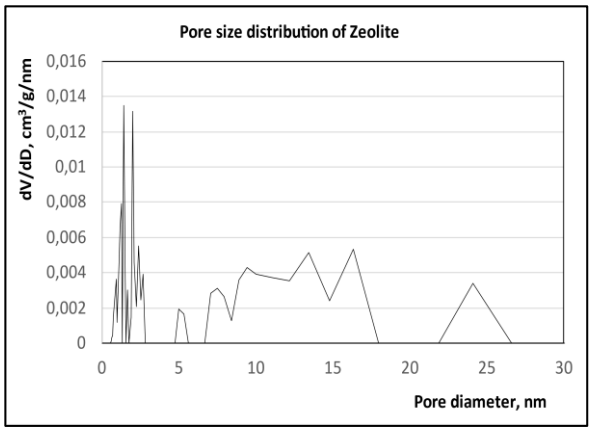

Fig. 8. Pore size distribution of zeolite.

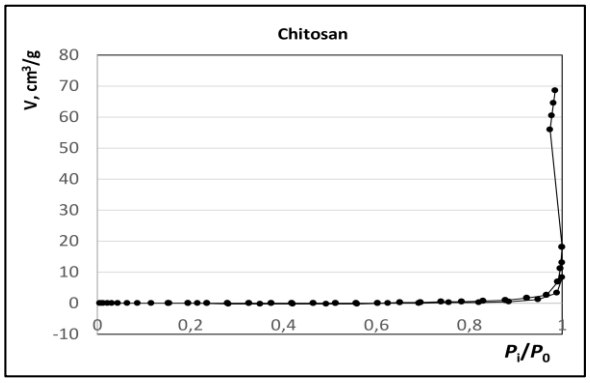

Fig 9. N_2 adsorption isotherms of chitosan.

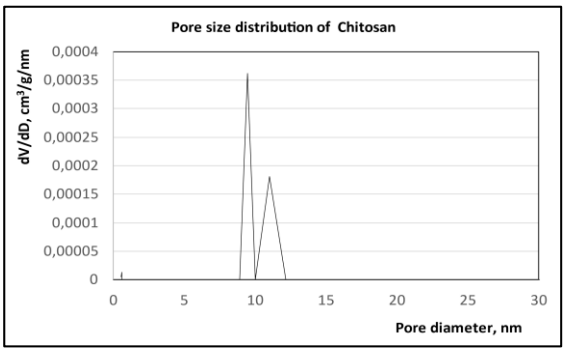

Fig. 10. Pore size distribution of chitosan.

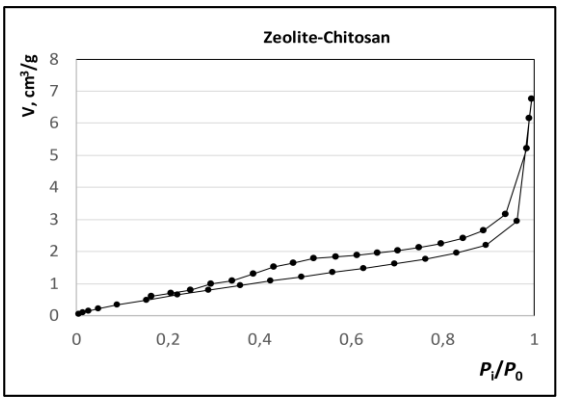

Fig 11. N_2 adsorption isotherms of zeolite - chitosan.

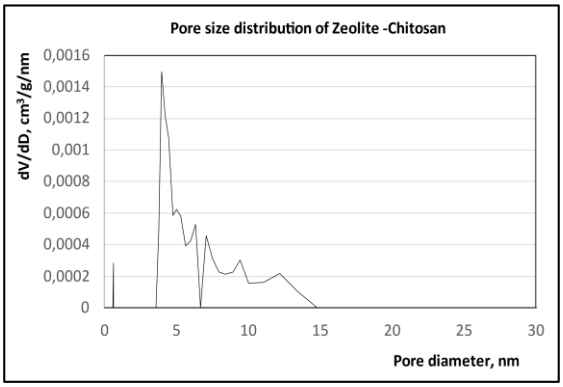

Fig. 12. Pore size distribution of zeolite - chitosan.

It should be mentioned that thermal destruction at proper experimental conditions of the samples leads to the production of materials that are highly dispersed with a well-developed system of pores and capillaries. Typically, the structure of a newly obtained pyrolytic product, i. e. char, retains the structure of the parental material as the formed pores are being oriented in a preferred direction corresponding to that of the precursor. This phenomenon is called *pseudomorphism*. It is the reason to observe the aforementioned peculiarities of the investigated chars.

Table 2. Textural analysis of chitosan, zeolite and chitosan–zeolite composite

Sample	CS	Z	CSZ
$V_{0.98}$ (cm^3 g^{-1})	0.0046	0.0964	0.0238
S_{BET} (m^2 g^{-1})	2	25	5
C	11.7	824.5	15.94
$V_{DR,\ micro}$ (cm^3 g^{-1})	0.0002	0.0103	0.0013
V_{meso}* (cm^3 g^{-1})	0.0044	0.0861	0.0225
$V_{DR,\ micro}$ (%)	4	11	5
V_{mezo} (%)	96	89	95
L_0 (nm)	9.44	1.41	2.82
	11.03	2.00	3.16
		1.26	4.73
		2.37	7.50
		13.41	9.44
		24.11	12.16

The textural analysis (Table 2) confirms that pristine zeolite possesses a highly developed porous structure, typical for clinoptilolite-rich materials. Its narrow micropores and broader mesopores contribute to its large surface area and make it suitable for sorption-based applications. In contrast, the pure chitosan sample demonstrated a significantly lower surface area and total pore volume, consistent with its polymeric, non-porous nature. Nonetheless, its pore volume was almost entirely mesoporous, suggesting a limited but accessible network, likely formed during membrane preparation and drying. The CSZ composite exhibits a moderate increase in both surface area and pore volume compared to pure chitosan. The presence of zeolite in the polymer matrix not only contributes to the formation of additional mesopores but also prevents structural collapse during drying. The resulting material benefits from the stabilizing effect of zeolite while retaining the flexibility of the biopolymer. The pore size distribution of CSZ reveals several mesopore populations, with dominant diameters in the range of 2.8–12.2 nm, confirming its hybrid nature.

The table presents the textural characteristics of the three samples — CS, Z, and CSZ. All materials exhibit relatively low values of specific surface area and total pore volume, indicating a limited development of the porous structure. Among them, sample Z shows the highest values of SBET (25 m^2/g) and V0.98 (0.0964 cm^3/g), suggesting a partially developed mesoporosity. Sample CS displays the lowest values of the porosity parameters, while the composite CSZ occupies an intermediate position, combining features of both precursor materials. The pore size distribution reveals that mesopores dominate in all samples, accounting for a substantial proportion (89–96%), whereas the fraction of micropores remains low. The average pore sizes (L_0) confirm this trend: sample Z exhibits smaller pores (1.4–3.7 nm), while CS and CSZ show larger pore dimensions in a wider range.

The conducted experiments clarify the nature and types of mechanophysical structures in the formation of pure chitosan and chitosan/zeolite composite biofilms, aiming to create a structure suitable for the incorporation of antibiotics on their surfaces. It was found that pure chitosan biofilms do not possess true physical porosity and belong to the so-called gel structural type, whereas chitosan/zeolite nanocomposite biofilms exhibit a textured morphology with developed physical porosity and, accordingly, a specific surface on which a relatively larger amount of drugs could potentially be implanted. Chemical composition analyses were performed using an X-ray microanalyzer (XMA), which revealed the presence of Al, Si, and Fe in the structure of the chitosan/zeolite nanocomposite biofilms. This feature enables the creation of a structure with genuine mechanophysical porosity and a well-developed specific surface, which is clearly advantageous for the implantation of antibiotics onto the internal surface of this type of drug carrier.

CONCLUSIONS

Because of their functional properties, chitosan/zeolite composites frequently exhibit remarkably improved mechanical strength; higher thermal stability, and relatively a good surface area [16-19]. Although the materials exhibit a limited development of surface area, they display varying degrees of porosity, with sample Z showing a relatively more pronounced porous structure. The composite sample CSZ combines the properties of CS and Z, which may provide a basis for balanced performance in applications that depend not so much on surface area as on chemical composition and the nature of active surface sites.

In addition to these characteristics, CSZ composites show the remarkable advantage of exhibiting biodegradability and biocompatibility associated with the biopolymer and thus can be an effective adsorbent due to its functional properties to remove pollutants.

Although the overall surface area of the composite does not reach that of the zeolite, the observed enhancement compared to chitosan alone demonstrates the synergistic interaction between the

two components. This structural modification may be advantageous in applications where moderate porosity, biocompatibility and mechanical reinforcement are required.

REFERENCES

1. V. E. Santo, M. E. Gomes, J. F. Mano, R. L. Reis, *J. Tissue Eng. Regen. Med*., **6**, (S3), s47 (2012) DOI: https://doi.org/10.1002/term.1519.
2. E. Vunain, A. Mishra, B. Mamba, *Int. J. Biol. Macromol.*, **86**, 570 (2016) DOI: https://doi.org/10.1016/j.ijbiomac.2016.02.005.
3. T. Anirudhan, S. Rijith, *J. Environ. Radioact*., **106**, 8 (2012) DOI: https://doi.org/10.1016/j.jenvrad.2011.10.013.
4. P. Grzybek, Ł. Jakubski, G. Dudek, *International Journal of Molecular Sciences,* **23**, 17 (2022) DOI: https://doi.org/10.3390/ijms23179932.
5. S. Kumar, R. Bera, N. Das, J. Koh, *Carbohydrate Polymers*, 232 (2020) DOI: https://doi.org/10.1016/j.carbpol.2019.115808.
6. M. Batista, M. L. Pinto, F. Antunes, J. Pires, S. Carvalho, *Materials*, **14,** 21, 6701 (2021) DOI: https://doi.org/10.3390/ma14216701.
7. L. Qiao, L. Zhao, C. Liang, K. Du, *J. Mater. Chem. B*, **7**, 5510 (2019).
8. T. M. Budnyak, I. V. Pylypchuk, V. A. Tertykh, E. S. Yanovska, D. Kolodynska Budnyak, *Nanoscale Research Letters*, **10** (87), 1 (2015) DOI: 10.1186/s11671-014-0722-1, 2014, DOI:10.1186/s11671-014-0722-1.
9. C. Bothiraja, U. Thorat, A. Pawar, K. Shaikh, *Mater. Technol*., **29**, (sup3), part B2, B120 (2014) DOI: https://doi.org/10.1179/1753555714Y.0000000174.
10. C. Viseras, C. Aguzzi, P. Cerezo, M. Bedmar, *Mater. Sci. Technol.*, **24** (9), 1020 (2008) DOI: https://doi.org/10.1179/174328408X341708.
11. F. Chivrac, E. Pollet, M. Schmutz, L. Avérous, *Carbohydr. Polym*., **80** (1), 145 (2010) DOI: https://doi.org/10.1016/j.carbpol.2009.11.004.
12. L. Alves, E. Ferraz, J. Gamelas, *Adv. Colloid Interf. Sci*., **272**, 101994 (2019), DOI: https://doi.org/10.1016/j.cis.2019.101994.
13. M. R. Abukhadra, A. Adlii, B. M. Bakry, *Int. J. Biol. Macromol*., **126**, 402 (2019) DOI: https://doi.org/10.1016/j.ijbiomac.2018.12.225
14. S. S. Ray, M. Okamoto, *Prog. Polym. Sci*., **28** (11), 1539 (2003), DOI: https://doi.org/
15. M. L. P. Dalida, A. F. V. Mariano, C. M. Futalan, C.-C. Kan, W.-C. Tsai, M.-W. Wan, *Desalination*, **275** (1–3), 154 (2011) DOI: https://doi.org/10.1016/j.desal.2011.02.051.
16. W.-C. Tsai, S. Ibarra-Buscano, C.-C. Kan, C.M. Futalan, M. L. P. Dalida, M.-W. Wan, *Desalin. Water Treat.*, **57** (21), 9799 (2016) DOI: https://doi.org/10.1080/19443994.2015.1035676.
17. W. S. Wan Ngah, N. F. M. Ariff, A. Hashim, M. A. K. M. Hanafiah, *Clean–Soil, Air, Water*, **38** (4), 394 (2010) DOI: https://doi.org/10.1002/clen.200900251.
18. K.-H. Liu, T.-Y. Liu, S.-Y. Chen, D.-M. Liu, *Acta Biomater*., **4**, 1038 (2008) DOI: https://doi.org/10.1016/j.actbio.2008.01.012.
19. S. Hua, H. Yang, W. Wang, A. Wang, *Appl. Clay Sci*., **50** (1), 112 (2010) DOI: https://doi.org/10.1016/j.clay.2010.07.012.